

DUAL FOUCAULT PENDULUM GYROSCOPE

D. Senkal, A. Efimovskaya, and A.M. Shkel

MicroSystems Laboratory, University of California, Irvine, CA, USA

ABSTRACT

We report a new type of MEMS degenerate mode lumped mass gyroscope architecture. The Dual Foucault Pendulum (DFP) gyroscope consists of two dynamically equivalent, mechanically coupled proof masses, oscillating in anti-phase motion. This dual axis tuning fork behavior creates a dynamically balanced resonator with x-y symmetry in frequency and damping. Phase synchronization is established by mechanical coupling of the two proof masses, whereas quadrature suppression is achieved by four differential shuttle pairs placed in-between. Dual axis tuning fork behavior provides vibration immunity and anchor loss mitigation, resulting in a Q-factor over 300,000 on both modes at a center frequency of 3.2 kHz. Due to high-Q degenerate mode operation, open-loop performance of $0.003^\circ/\sqrt{\text{h}}$ ARW and $0.27^\circ/\text{h}$ in-run bias stability were experimentally demonstrated. We believe Dual Foucault Pendulum is the minimal realization of a dynamically balanced lumped mass degenerate mode gyroscope.

INTRODUCTION

Coriolis Vibratory Gyroscopes (CVGs) can be divided into two categories [1]: Non-degenerate mode gyroscopes which are designed intentionally to be asymmetric in x and y modes ($\Delta f \neq 0$) and degenerate mode gyroscopes which have x-y symmetry ($\Delta f = 0$). Degenerate mode CVGs have potential advantages over non-degenerate mode CVGs in terms of rate sensitivity and potential to implement whole angle mechanization and self-calibration.

Due to these potential advantages, many MEMS degenerate mode gyroscope architectures emerged in the recent years. These architectures can be broadly divided into 3 categories: (1) 3-D micro-wineglass gyroscopes, (2) ring/disk gyroscopes, and (3) lumped mass systems. 3-D micro-wineglass gyroscopes typically combine 3-D fabrication techniques with low internal loss materials, such as micro-glassblown [2] and blow torch molded [3] fused silica wineglasses or surface micro-machined poly-diamond resonators [4]. Whereas ring/disk gyroscopes aim to mimic the behavior of wineglass gyroscopes using 2-D micro-machined structures, examples include ring [5] or disk gyroscopes [6] as well as concentric ring systems [7, 8]. Finally, lumped mass systems utilize more conventional micro-machining elements, such as proof masses, folded beam suspensions, and comb fingers. Examples include single-mass systems such as [9] or multi-mass systems such as the Quadruple Mass Gyroscope (QMG) [10]. All of these architectures have a potential for achieving high performance due to degenerate mode operation. However, the implementation requires either challenging fabrication processes or complex mechanical systems.

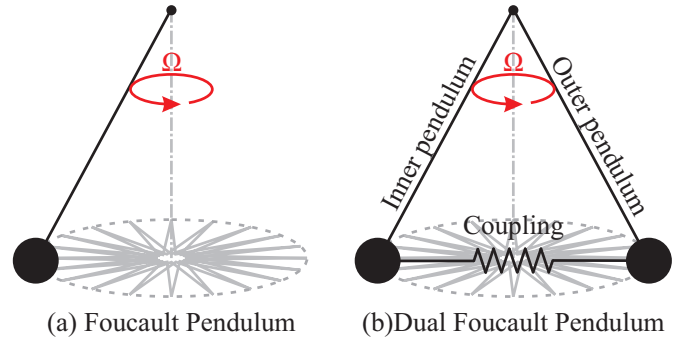


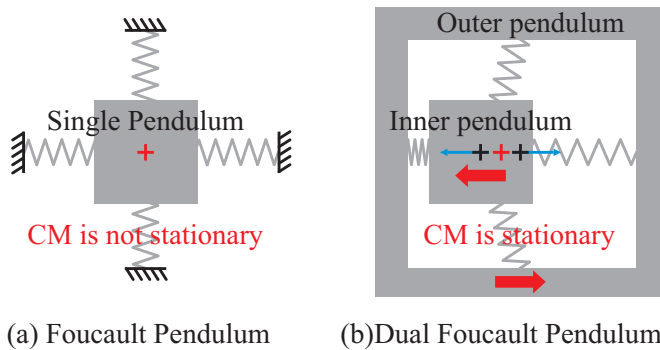
Figure 1: Dual Foucault Pendulum (DFP) gyroscope consists of two mechanically coupled Foucault Pendulums.

In this work, we are exploring a new gyro architecture that combines simplicity and dynamic balance of tuning fork gyros [11] (two mass anti-phase motion) with high rate sensitivity of degenerate mode gyroscopes (x-y symmetry). Core of the gyroscope architecture is two mechanically coupled and dynamically equivalent proof masses, oscillating in anti-phase motion, Fig. 1(b). Each proof mass is free to swing in any direction on the x-y plane, analogous to a Foucault Pendulum, Fig. 1(a). However, unlike a conventional tuning fork gyroscope, center of masses of the two proof masses are aligned. This creates force and moment balance for both x and y modes, providing immunity to vibration and shock as well as anchor loss mitigation. We believe this two-mass architecture is the minimum lumped mass gyroscope configuration that can provide a dynamically balanced system in both x and y directions.

Whole angle mechanization and virtual carouseling of the Dual Foucault Pendulum Gyroscope (DFP) was presented in [12]. This paper focuses on design and fabrication of the sensor's mechanical element, integration into the experimental setup, and open loop/force-to-rebalance rate gyroscope operation.

DESIGN

Core of the Dual Foucault Pendulum (DFP) Gyroscope is two mechanically coupled and dynamically equivalent proof masses, oscillating in anti-phase motion. Dynamic balance is obtained by aligning the center of masses of each proof mass. This allows the center of mass of the system to remain stationary during oscillation, causing the net force and torques generated by the combined system to be zero at all times, Fig. 2. Unlike a conventional tuning fork gyroscope, the force and torque balance is obtained on both x and y modes of the gyroscope.



(a) Foucault Pendulum (b) Dual Foucault Pendulum
 Figure 2: Vibration immunity and anchor loss mitigation are provided by anti-phase operation of two dynamically equivalent Foucault Pendulums.

In our implementation, dynamic equivalence of the two proof masses is achieved by using identical (mirrored) suspension elements and shuttle assemblies, while designing the two proof masses to have equal masses. This results in same resonance frequencies for individual proof masses, which is further reinforced by mechanical coupling of the two proof masses. This mechanical coupling is achieved via "weak springs" between shuttle assemblies of inner and outer proof masses, which synchronizes the phases of the proof masses, Fig. 3.

There are four shuttle pairs within the gyroscope. Each shuttle pair is connected to both inner and outer proof masses and can only move in one direction. This helps mitigate cross-axis coupling between the x and y modes by restricting electrode movement in one direction. During gyroscope operation, for each x and y mode, two shuttle pairs remain parked, whereas the other two shuttles oscillate in anti-phase motion together with their respective proof masses.

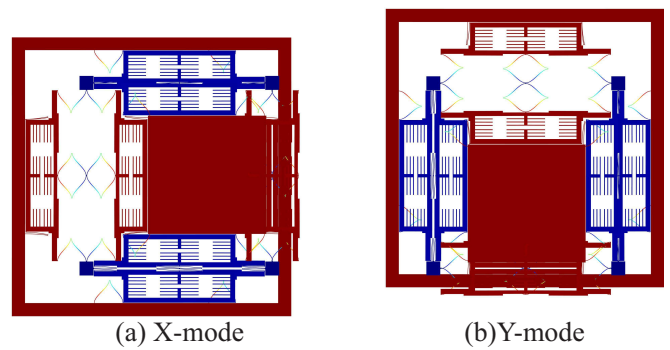
Electrostatic transduction is provided by arrays of parallel plates located on the shuttle assemblies. In order to achieve large displacements necessary for low noise operation, 8 μm capacitive gaps are used on the parallel plates. Large free space between the two proof masses allows placement of 12 layers of parallel plate electrodes per shuttle pair, resulting in over 12.5 pF total capacitance ($dC/dx = 1.5 \mu\text{F/m}$).

Device is suspended from 4 anchors placed in between the two proof masses. Each anchor is shared by one x and one y shuttle pair. To help protect the mechanical element from unwanted packaging stresses, attachment of the gyroscope die to the package is done in between the 4 anchors, via a central attachment point.

EXPERIMENTAL RESULTS

Fabrication

Device was fabricated on a standard SOI process, with a footprint of 6700 μm × 6700 μm, Fig 4. A device layer of 100 μm and a buried oxide layer of 5 μm were used. AZ 4620 photoresist and conventional contact lithography was used to define the sensor features. DRIE etching of the device layer was done in a STS DRIE system, which was followed by a



(a) X-mode (b) Y-mode
 Figure 3: FEA showing x-y symmetric anti-phase operation. Device is anchored at four points in between the proof masses. Colors correspond to total displacement.

HF release step using an Idonus Vapor Phase Etcher. After dicing, individual dies were attached to 44 pin ceramic LCC packages and wirebonded for characterization.

Front-end Electronics

A low-outgassing ceramic PCB was used for front-end electronics. First stage amplification of the gyroscope output was done using dual trans-impedance amplifiers (Analog Devices AD8066) with 1 MΩ gain resistors and 2.2 pF capacitors. Output of the transimpedance amplifiers were cascaded into an instrumentation amplifier (Analog Devices AD8429).

The same instrumentation amplifiers (Analog Devices AD8429) were also used for forcer electronics. Unity gain was used on the forcer electronics due to extremely low voltage levels required to drive the gyroscope (less than 1 mV). DC biasing was done only on the forcer electrodes and the resonator.

Finally, low dropout voltage regulators (Texas Instruments TPS7A3001 and TPS7A4901) were used for supplying power to the active components on the PCB. These helped to reduce system noise by rejecting a large portion of the power supply noise.

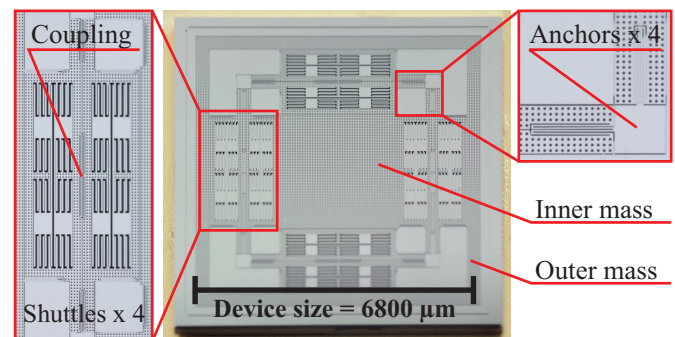


Figure 4: Image of fabricated gyroscope with a closeups of the shuttle assemblies and the anchors.

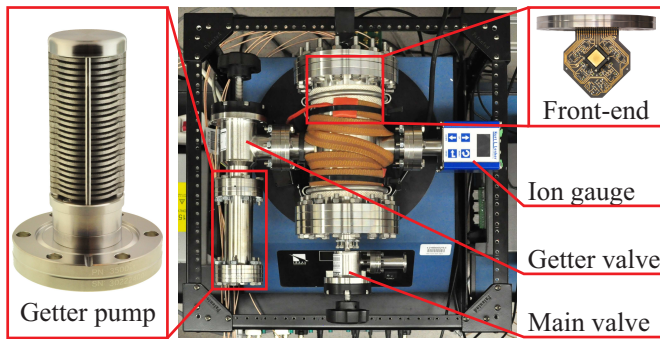


Figure 5: High-vacuum test-bed with non-evaporable getter pump provides μTorr level vacuum for rate characterization.

Experimental Setup

A high-vacuum test-bed was used for gyro characterization, Fig. 5. The test-bed consists of four main components:

- Low-outgassing ceramic PCB front-end electronics,
- Macro-scale non-evaporable getter pump,
- Stainless steel vacuum chamber assembly,
- Rate table with slip rings.

For rate table characterization, the device is mounted onto the front-end PCB and inserted into the vacuum chamber assembly. Electrical feed-through from the vacuum chamber is provided by a 37 pin D-SUB connector, which is then routed through the slip rings. Angle valve is used to seal the getter pump, during insertion of the device into the vacuum chamber. Another angle valve is used to seal the entire vacuum chamber, so that the external turbo pump can be disconnected for continuous 360° rotation of the rate table.

After the system is pumped down using an external turbo pump, the non-evaporable getter pump is activated using the internal resistive heater and the chamber is sealed off. Due to the large absorption capacity of the getter pump and the low-outgassing ceramic front-end electronics, the system can sustain high vacuum without the need for active pumping. This eliminates unwanted vibrations caused by rotary pump systems and permits continuous 360° rotation of the rate table at sustained vacuum levels of $< 10 \mu\text{Torr}$.

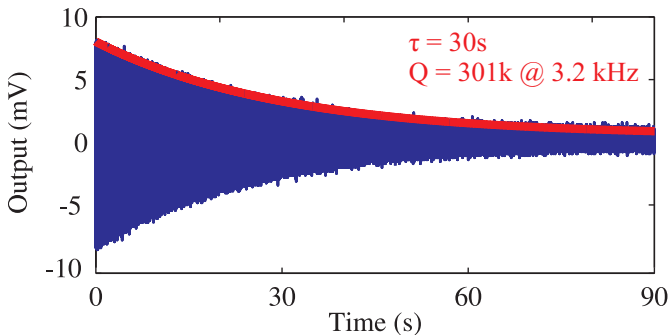


Figure 6: Ring down experiment showing energy decay time constant (τ) of 30 s or Q of 301k at 3.2 kHz.

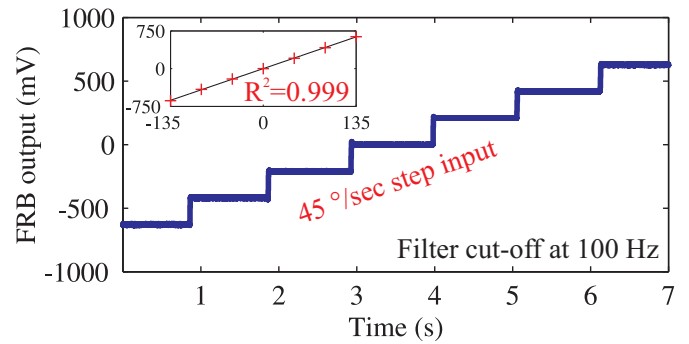


Figure 7: Rate characterization with $45^\circ/\text{s}$ step input showed a FRB scale factor of $4.66 \text{ mV}/(^\circ/\text{s})$, goodness of fit: $R^2 = 0.999$.

Rate Gyroscope Operation

Ring-down characterization was used to measure the Q-factor of the mechanical element at a vacuum level of $< 10 \mu\text{Torr}$. An exponential curve fit to the ring-down data, showed an energy decay time constant (τ) of 30 s at 3.2 kHz, which corresponds to Q-factor over 300,000, Fig. 6.

An as-fabricated frequency split (Δf) of 18 Hz was observed, which was later electrostatically tuned to $< 100 \text{ mHz}$ by biasing the forcer electrodes. This was achieved by applying a DC bias of 10 V DC at the resonator, while applying 9 V DC to the x forcer electrodes and -6.75 V DC to the y forcer electrodes. Lower DC bias voltages can be used if pick-off electrodes in addition to the forcer electrodes are used for electrostatic tuning.

After electrostatic tuning, Phase Locked Loop (PLL), Amplitude Gain Control (AGC) and Quadrature Null loops were implemented on a Zurich HF2LI lock-in amplifier [13]. PLL was locked to the drive mode and AGC was used to stabilize the drive amplitude. In the experiments, an AC quadrature null loop was utilized, where the sense mode forcer electrodes were used to drive the quadrature output of the sense mode to zero. Device was tested with both open-loop and force-to-rebalance configurations.

Scale factor characterization was done using continuous rotation of the rate table and incrementally changing the angular velocity. A linear fit to the gyro output was used to extract the scale factor. An open-loop scale factor of $26.4 \text{ mV}/(^\circ/\text{s})$ and force-to-rebalance scale factor of $4.66 \text{ mV}/(^\circ/\text{s})$ were measured with a goodness of fit: $R^2 = 0.999$, Fig. 7. After the scale factor was obtained, Allan variance analysis of the gyroscope zero rate output was performed for both open-loop and force-to-rebalance operation, Fig. 8. No temperature stabilization or compensation was used during the experiment. For open-loop operation, angle random walk (ARW) of $0.003^\circ/\sqrt{\text{h}}$ and an in-run bias stability of $0.27^\circ/\text{h}$ were measured. Whereas for FRB configuration an ARW of $0.06^\circ/\sqrt{\text{h}}$ and bias stability of $1.5^\circ/\text{h}$ were measured. Higher ARW in FRB operation was associated with feedback noise from the digital to analog converters (DACs).

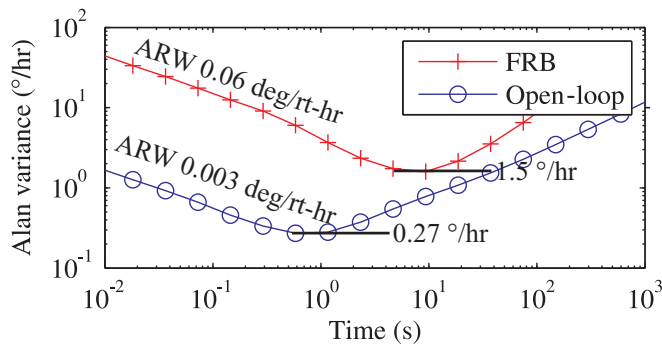


Figure 8: Alan variance of zero rate output, showing ARW and in-run bias instability for FRB and open-loop operation.

CONCLUSIONS

A new type of MEMS degenerate mode gyroscope is presented. Dual Foucault Pendulum (DFP) Gyroscope aims to combine dynamic balance of tuning fork gyroscopes with high rate sensitivity and rate integrating capability of high quality factor degenerate mode gyroscopes, in a minimal (two-mass) configuration. Ring-down characterization of the mechanical element at a vacuum level of $5\ \mu\text{Torr}$ showed an energy decay time constant (τ) of 30 s at 3.2 kHz, which corresponds to Q-factor over 300,000 on both modes. Initial characterization of open-loop gyro performance at zero rate showed angle random walk (ARW) of $0.003^\circ/\sqrt{\text{h}}$ and an in-run bias stability of $0.27^\circ/\text{h}$. Whereas FRB operation showed higher noise with an ARW of $0.06^\circ/\sqrt{\text{h}}$ and bias stability of $1.5^\circ/\text{h}$, which was associated with feedback noise from the digital to analog converters (DACs).

We believe, Dual Foucault Pendulum (DFP) is the minimal realization of a dynamically balanced lumped mass gyroscope. Combination of a simple gyro architecture and high-Q degenerate mode operation may potentially lead to low-cost, high performance MEMS gyroscopes.

ACKNOWLEDGEMENTS

This material is based upon work supported by DARPA micro-PNT program (Program Manager Dr. Robert Lutwak). Design and characterization was done in UCI Microsystems Laboratory. Fabrication was done at UCI INRF facility. Authors would like to acknowledge Sina Askari for his help in PCB fabrication and assembly.

REFERENCES

- [1] A M Shkel. Type I and Type II Micromachined Vibratory Gyroscopes. In *IEEE/ION Position Location and Navigation Symposium (PLANS)*, pages 586–593, San Diego, California, USA, 2006.
- [2] D Senkal, M J Ahamed, S Askari, and A M Shkel. 1 Million Q-Factor Demonstrated on Micro-glassblown Fused Silica Wineglass Resonators with Out-of-Plane Electrostatic Transduction. In *Solid-State Sensors, Actuators and Microsystems Workshop (Hilton Head)*, pages 68–71, Hilton Head Island, South Carolina, USA, 2014.

- [3] J Cho, T Nagourney, A Darvishian, B Shiari, J Woo, and K Najafi. Fused Silica Micro Birdbath Shell Resonators with 1.2 Million Q and 43 Second Decay Time Constant. In *Solid-State Sensors, Actuators and Microsystems Workshop (Hilton Head)*, pages 103–104, Hilton Head Island, South Carolina, USA, 2014.
- [4] D Saito, Chen Yang, Amir Heidari, Hadi Najari, Liwei Lin, and David A Horsley. Batch-Fabricated High Q-Factor Microcrystalline Diamond Cylindrical Resonator. In *IEEE International Conference on Micro Electro Mechanical Systems (MEMS)*, pages 801–804, Estoril, Portugal, 2015.
- [5] Farrokh Ayazi and Khalil Najafi. A HARPSS Polysilicon Vibrating Ring Gyroscope. *Journal of Microelectromechanical Systems*, 10(2):169–179, 2001.
- [6] Zhili Hao, Siavash Pourkamali, and Farrokh Ayazi. VHF Single-Crystal Silicon Elliptic Bulk-Mode Capacitive Disk Resonators-Part I: Design and Modeling. *Journal of Microelectromechanical Systems*, 13(6):1043–1053, 2004.
- [7] Anthony D Challoner, Howard H Ge, and John Y Liu. Boeing Disc Resonator Gyroscope. In *IEEE/ION Position Location and Navigation Symposium (PLANS)*, pages 504–514, Savannah, Georgia, USA, 2014.
- [8] D Senkal, S Askari, M J Ahamed, E J Ng, V Hong, Y Yang, C H Ahn, T W Kenny, and A M Shkel. 100k Q-Factor Toroidal Ring Gyroscope Implemented in Wafer-Level Epitaxial Silicon Encapsulation Process. In *IEEE International Conference on Micro Electro Mechanical Systems (MEMS)*, pages 9–12, Taipei, Taiwan, 2014.
- [9] Congzhong Guo, Erdinc Tatar, and Gary K. Fedder. Large-Displacement Parametric Resonance Using a Shaped Comb Drive. In *IEEE International Conference on Micro Electro Mechanical Systems (MEMS)*, pages 173–176, Taipei, Taiwan, 2013.
- [10] A A Trusov, G Atikyan, D M Rozelle, A D Meyer, S A Zotov, B R Simon, and A M Shkel. Flat is not dead: Current and future performance of Si-MEMS Quad Mass Gyro (QMG) system. In *IEEE/ION Position Location and Navigation Symposium (PLANS)*, pages 252–258, Savannah, Georgia, USA, May 2014.
- [11] J Bernstein, S Cho, A T King, P Kourepenis, P Maciel, and M Wienberg. A Micromachined Comb-Drive Tuning Fork Rate Gyroscope. In *IEEE International Conference on Micro Electro Mechanical Systems (MEMS)*, pages 143–148, Fort Lauderdale, Florida, USA, 1993.
- [12] D Senkal, A Efimovskaya, and A M Shkel. Minimal Realization of Dynamically Balanced Lumped Mass WA Gyroscope: Dual Foucault Pendulum. In *IEEE/ASME International Symposium on Inertial Sensors and Systems*, pages 131–134, Kohala Coast, Hawaii, USA, 2015.
- [13] D D Lynch. Coriolis Vibratory Gyros. In *Symposium Gyro Technology*, Stuttgart, Germany, 1998.

CONTACT

* D. Senkal, tel: +1-949-945-0858; doruksenkal@gmail.com